Preprints of the 21st IFAC World Congress (Virtual)
Berlin, Germany, July 12-17, 2020

State Affine Modeling and Observer Design for Hall-Héroult Process ⋆

Lucas José da Silva Moreira * **Mirko Fiacchini** *
Gildas Besançon * **Francesco Ferrante** * **Hervé Roustan** **

* *Univ. Grenoble Alpes, CNRS, Grenoble INP, GIPSA-lab, Grenoble, France. (e-mail: lucas-jose.da-silva-moreira, mirko.fiacchini , gildas.besancon, francesco.ferrante @grenoble-inp.fr).*
** *Rio Tinto, Laboratoire de Recherche des Fabrications, Saint Jean de Maurienne, France(e-mail: herve.roustan@riotinto.com)*

Abstract: Hall-Héroult process is a complex electrolysis procedure to produce aluminum. Due to the extreme operational conditions, it is difficult to continuously measure certain important values. This paper presents an approach to model and estimate the alumina concentration and anode-cathode distance based on the available measurements. Initially, a state affine model is obtained using a combination of physical-chemical relations and system identification. Then, a linear Kalman observer is designed to recover the desired signals. The proposed approach is validated on an industrial platform.

Keywords: Aluminum electrolysis, modeling, state estimation, Kalman filter

1. INTRODUCTION

Hall-Héroult process is the electrolysis method to produce aluminum at industrial scale (Grjotheim and Welch, 1980). In short, it is based on an electrochemical reaction that requires the dissolution of alumina (Al_2O_3) in molten cryolite bath under a high-temperature condition. During the electrolysis process, carbon anodes are dipped in the solution, while the produced liquid aluminum is accumulated at the bottom of the cell and carbon dioxide gas is expelled out of the system. The process is summarized by the following chemical equation:

$$Al_2O_{3(diss)} + \frac{3}{2}C_{(anode)} \rightarrow 2Al_{(l)} + \frac{3}{2}CO_{2(g)} \qquad (1)$$

In large industrial plants, each cell has a large number of anodes connected in parallel and supported by a common busbar. The height of this bar can be set during the operation to adjust the anode-cathode distance (ACD). High DC current, in the order of kilo-amps, is applied to each anode. This large intensity is required to increase the amount of aluminum produced. The chemical reagent, alumina, is periodically injected into the system as powder by feeders along with the pot cell. A simple schematic view of a Hall-Héroult cell is shown in Figure 1.

The hazardous conditions inside the pot such as high temperature, magnetic field and the presence of corrosive elements, make it difficult to develop sensors for continuous measurement. Moreover, some important state variables of the process are not measured at any time during the operation. This inconvenient can lead to inaccurate results (Jakobsen et al., 2001) and it restrains the process production efficiency (Yao and Bao, 2018).

⋆ This research was partially supported by project PIANO.

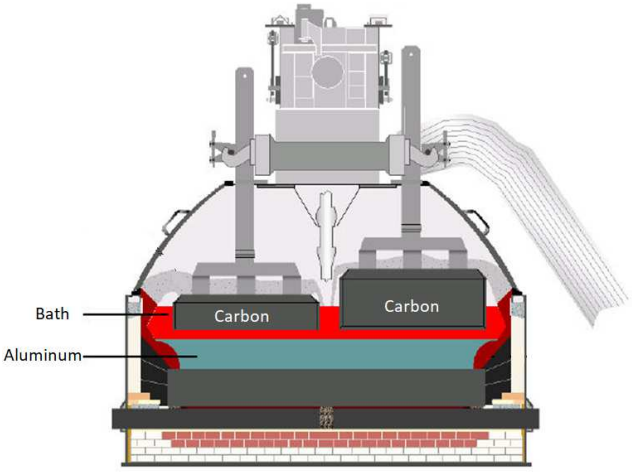

Fig. 1. Pot Schematic View

Some researchers have been developing nonlinear estimators to overcome this information limitation and obtain the desired process states (Kolås et al., 2008; Jakobsen et al., 2001; Hestetun and Hovd, 2005). However, those works are mostly based on the approximate *Extended Kalman Filter* (Moore and Anderson, 1979), and do say not much about the underlying physics.

The present paper aims to provide a simple model for the Hall-Héroult process, yet capturing the main features of a regular operation by combining physical-chemical aspects with experimental models. In continuation of the work developed in (da Silva Moreira et al., 2020), the system is modeled in a *state affine* form, so as to allow an observer implementation here using *exact* Linear Kalman results, in the spirit of (Ţiclea and Besançon, 2013) for instance. An identification procedure for a first model

calibration is then presented. This procedure is validated with operational collected data and tested for different conditions in APX pot cell of Rio Tinto *Laboratoire des Recherches de Fabrications* (LRF) located in Saint Jean de Maurienne, France. For confidentiality reasons, the data in the y-axis in all plots have been removed.

The paper goes on as follows: section 2 gives an overview of the problem we consider, section 3 presents the modeling that we propose, and section 4 provides online state estimation implementation and results. Some conclusions are summarized in section 5.

2. PROBLEM DESCRIPTION

The process efficiency is directly related to the distance gap between the cathode and anode, (ACD) (Côté et al., 2017). This value is not constant during the operation due to the chemical reaction. The carbon anodes are consumed and they are replaced after some time. Moreover, the liquid aluminum layer increases its height because of the production. Furthermore, current perturbations and bath composition can also affect the ACD. However, the hazardous conditions inside the pot make it impossible to develop a sensor for continuous measurement. The ACD is critical since a large distance decreases the pot cell production and a small value can cause a short-circuit between the produced aluminum and the anode (Keniry et al., 2001). Unfortunately, only a few papers have modeled this dynamical behavior (Jakobsen et al., 2001; Yao et al., 2017).

The dissolved alumina concentration (wAl_2O_3) is also an important quantity that is not continuously measured. Commonly, just a few samples per week are manually taken, which makes it difficult to obtain an experimental model. This quantity is again very important: A low concentration triggers the so-called "anode effect" (Bearne, 1999) which can cause interruptions on the production and produces greenhouse gases. Conversely, a high concentration makes it possible to see sludge formation.

In practice, only the line current (I), line voltage (V), the busbar position (BM), and the frequency of the alumina feeding (F) are continuously collected by sensors. For the system regulation, an indirect measurement called the pseudo-resistance (R) is commonly used to adjust the ACD and wAl_2O_3. It is calculated according to the following formula:

$$R(t) = \frac{V(t) - V_{ext}}{I(t)} \tag{2}$$

where V_{ext} is the voltage intercept of cell voltage versus current extrapolated from a small change in current to zero current.

Based on the pseudo-resistance value, the alumina feeding frequency is modified. It alternates between two predetermined periods to have faster or slower feeding. This value is adjusted by the ACD regulation to ensure control stability and obtain a good current efficiency (Homsi et al., 2016). A nonlinear relation between R, ACD and wAl_2O_3 is also known to take the form of Fig. 2 (Haupin, 2016). From this complex relation, it is not easy to obtain some information. All this motivates the development of a model for the unknown state dynamics, and an observer to get an online estimation for it.

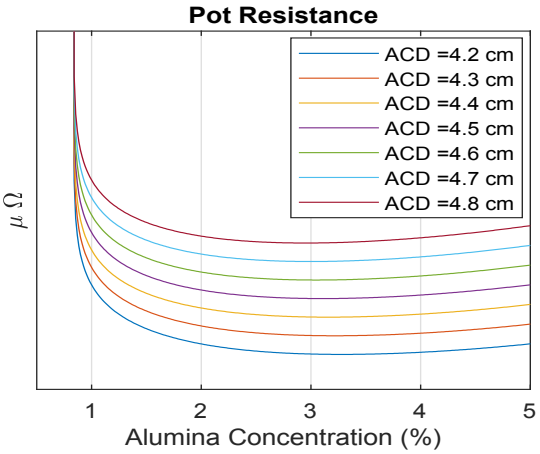

Fig. 2. Typical pot resistance curve as function of alumina concentration and ACD

3. MODELING

The aim of this section is to obtain a discrete-time model that explicitly relates ACD and wAl_2O_3 to the pot pseudo-resistance R. The model is obtained using a hybrid approach that combines physical-chemical aspects and information extracted from data.

3.1 Anode-Cathode Distance

From the problem description, it is possible to define the ACD variation ($\frac{d}{dt}ACD$) as the height variation between the aluminum ($\frac{d}{dt}Al_{height}$) and carbon ($\frac{d}{dt}C_{height}$) layers, plus the anodes busbar beam movement ($\frac{d}{dt}BM$):

$$\frac{d}{dt}ACD(t) = \frac{d}{dt}Al_{height}(t) - \frac{d}{dt}C_{height}(t) + \frac{d}{dt}BM(t) \tag{3}$$

Each element height can be written as a function of the mass production by the density relation. Hence, the aluminum and carbon height variation become:

$$\frac{d}{dt}Al_{height}(t) = \frac{1}{\rho_{Al}S}\left[\frac{d}{dt}m_{Al}(t)\right] \tag{4}$$

$$\frac{d}{dt}C_{height}(t) = \frac{1}{\rho_{C}S}\left[\frac{d}{dt}m_{C}(t)\right] \tag{5}$$

where ρ_{Al} is the liquid aluminum density, m_{Al} is the aluminum produced mass, ρ_C is the carbon density, m_C is the carbon produced mass, and S is the average reaction surface area.

The produced aluminum mass rate ($\frac{d}{dt}m_{Al}$) is given by the Faraday's law of electrolysis:

$$\frac{d}{dt}m_{Al}(t) = \frac{C_e Al_m}{3\mathfrak{F}}I(t) \tag{6}$$

where C_e is the current efficiency, Al_m is the aluminum molar mass, $I(t)$ is the line current, $\mathfrak{F}$ is the Faraday's constant, and 3 is the valency number of ions of the aluminum given by:

$$4Al^{3+} + 6O^{2-} + 3C_{(anode)} \rightarrow 4Al_{(l)} + 3CO_{2(g)} \tag{7}$$

From the chemical balance of equation (1), it is possible to relate the aluminum mass production with the carbon

mass consumption. This leads to the carbon mass consumption rate $\frac{d}{dt}m_C$ formula:

$$\frac{d}{dt}m_C(t) = \frac{C_m}{4\mathfrak{F}}I(t) \tag{8}$$

where C_m is the carbon molar mass and 4 is the stoichiometric coefficient.

Hence, equation (3) can be rewritten using the above expressions:

$$\frac{d}{dt}ACD(t) = \frac{1}{S\mathfrak{F}}\left(\frac{C_e Al_m}{3\rho_{Al}} - \frac{C_m}{4\rho_C}\right)I(t) + \frac{d}{dt}BM(t) \tag{9}$$

The beam movement derivative is considered as one of the system inputs (u_1):

$$u_1(t) = \frac{d}{dt}BM(t) \tag{10}$$

Hence, by defining β as:

$$\beta = \frac{1}{S\mathfrak{F}}\left(\frac{C_e Al_m}{3\rho_{Al}} - \frac{C_m}{4\rho_C}\right) \tag{11}$$

And using equation (11) in (9), the ACD dynamics results:

$$\frac{d}{dt}ACD(t) = \beta I(t) + u_1(t) \tag{12}$$

Using Euler discretization in equation (12), it is possible to obtain a discrete-time model for the ACD:

$$ACD[n+1] = ACD[n] + T_s(u_1[n] + \beta I[n]) \tag{13}$$

where T_s is the sampling time.

As it is not possible to measure the ACD during the operation of the plant, β cannot be obtained experimentally. Hence, this parameter is calculated using theoretical values.

3.2 Alumina Concentration

The dynamics of alumina concentration wAl_2O_3 can be modeled as the difference between the quantity injected by the feeders (wAl_2O_{3in}) and the consumed by the chemical reaction (wAl_2O_{3cons}):

$$\frac{d}{dt}wAl_2O_3(t) = wAl_2O_{3in}(t) - wAl_2O_{3cons}(t) \tag{14}$$

The quantity injected by the feeders at time t can be represented by:

$$wAl_2O_{3in}(t) = \frac{Nm_{in}}{M}F(t) \tag{15}$$

where N is the number of feeders in the pot, m_{in} is the amount of mass injected by feeders, M is the total bath mass, and F is the frequency of feeders. The alumina injected in the system does not dissolve instantaneously. This effect can be approximated by a time delay D introduced in equation (15):

$$wAl_2O_{3in}(t) = \frac{Nm_{in}}{M}F(t-D) \tag{16}$$

The frequency of the feeders is considered as one of the system inputs (u_2):

$$u_2(t) = F(t-D) \tag{17}$$

Then, equation (16) becomes:

$$wAl_2O_{3in}(t) = \frac{Nm_{in}}{M}u_2(t) \tag{18}$$

The Al_2O_3 consumption is given by the Faraday's law divided by the bath mass:

$$wAl_2O_{3cons}(t) = \frac{Al_2O_{3m}C_e}{6\mathfrak{F}M}I(t) \tag{19}$$

where Al_2O_{3m} is the alumina molar mass and 6 is the number of electrons required for the electrolysis to perform.

Replacing equations (18) and (19) in (14):

$$\frac{d}{dt}wAl_2O_3(t) = \frac{Nm_{in}}{M}u_2(t) - \frac{Al_2O_{3m}C_e}{6\mathfrak{F}M}I(t) \tag{20}$$

And defining:

$$\alpha_1 = \frac{Nm_{in}}{M},\ \alpha_2 = \frac{Al_2O_{3m}C_e}{6\mathfrak{F}M} \tag{21}$$

Equation (20) can be written as:

$$\frac{d}{dt}wAl_2O_3(t) = \alpha_1 u_2(t) - \alpha_2 I(t) \tag{22}$$

Using Euler discretization in equation (22):

$$wAl_2O_3[n+1] = wAl_2O_3[n] + T_s(\alpha_1 u_2[n] - \alpha_2 I[n]) \tag{23}$$

Then, it is possible to obtain a discrete-time model for the alumina concentration. The next step is to identify parameters D, α_1 and α_2.

The time-delay is estimated as a result of an unconstrained nonlinear optimization problem. The cost function is defined as the mean square error between the resistance measurements and simulated values from a model using ACD and wAl_2O_3 values in many data sets. Then, the optimization searches the best time-delay to decrease fitting error.

Just a few alumina concentration measurements are recorded during an operational day without constant sampling time. It is possible to organize equation (23) in a matrix form as follows using the data collected at times $[\tau_0\ \tau_1\ \cdots\ \tau_N\ \tau_{N+1}]$:

$$\begin{bmatrix} wAl_2O_3(\tau_1) - wAl_2O_3(\tau_0) \\ wAl_2O_3(\tau_2) - wAl_2O_3(\tau_1) \\ \vdots \\ wAl_2O_3(\tau_{N+1}) - wAl_2O_3(\tau_N) \end{bmatrix} = T_s \begin{bmatrix} \sum_{k=\tau_0}^{\tau_1} u_2(k) & -\sum_{k=\tau_0}^{\tau_1} I(k) \\ \sum_{k=\tau_1}^{\tau_2} u_2(k) & -\sum_{k=\tau_1}^{\tau_2} I(k) \\ \vdots & \vdots \\ \sum_{k=\tau_{N-1}}^{\tau_N} u_2(k) & -\sum_{k=\tau_{N-1}}^{\tau_N} I(k) \end{bmatrix} \begin{bmatrix} \alpha_1 \\ \alpha_2 \end{bmatrix} \tag{24}$$

Based on this structure, it is possible to identify the parameters α_1 and α_2 by least square estimation. Fig. 3 shows a comparison between the model simulated with estimated parameters α_1 and α_2 and the alumina concentration values collected on the plant. The model is initialized with measurement and the simulation is started using the signals of u_2 and I. Every time a new alumina concentration measurement is available, the model

is reinitialized to improve the accuracy of the prediction provided by the model. Following this approach, the mean absolute relative error between the model outputs and the measurement is 3.52 %.

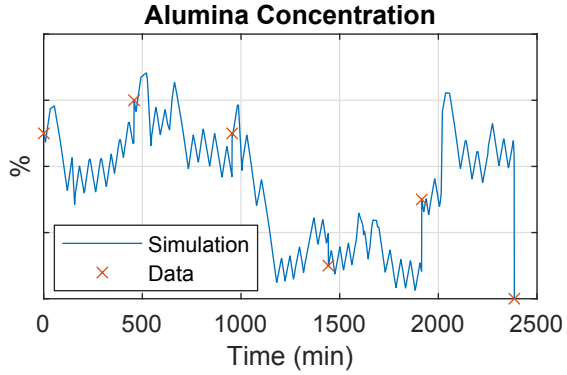

Fig. 3. Alumina Concentration Model Validation

3.3 Pseudo-Resistance

As for the pot pseudo-resistance, an approximate polynomial can be obtained from Fig. 2. Considering regular process operation in which alumina concentration varies between 2% and 4%, this model takes the following form:

$$R(t) = cwAl_2O_3^2(t) + (d + eACD(t))wAl_2O_3(t) + (f + gACD(t)) \tag{25}$$

where c, d, e, f, and g are some parameters to be determined. By differentiating the equation (25), the parameter f goes to zero and it is possible to obtain a dynamic behavior model for the pseudo-resistance:

$$\begin{aligned}\frac{d}{dt}R(t) = {} & eACD(t)\frac{d}{dt}wAl_2O_3(t) \\ & + \left(2c\frac{d}{dt}wAl_2O_3(t) + e\frac{d}{dt}ACD(t)\right)wAl_2O_3(t) \\ & + d\frac{d}{dt}wAl_2O_3(t) + g\frac{d}{dt}ACD(t)\end{aligned} \tag{26}$$

Using Euler discretization in equation (26), it is possible to obtain the resistance variation model:

$$\begin{aligned}R[n+1] = R[n] + T_s\,(& e\Delta wAl_2O_3[n]ACD[n] \\ & + (2c\Delta wAl_2O_3[n] + e\Delta ACD[n])wAl_2O_3[n] \\ & + d\Delta wAl_2O_3[n] + g\Delta ACD[n])\end{aligned} \tag{27}$$

where:

$$\Delta ACD[n] := \frac{ACD[n] - ACD[n-1]}{T_s} \tag{28}$$

$$\Delta wAl_2O_3[n] := \frac{wAl_2O_3[n] - wAl_2O_3[n-1]}{T_s} \tag{29}$$

Equations (28) and (29) can be respectively approximated by:

$$\Delta ACD[n] \approx u_1[n] + \beta I[n] \tag{30}$$

$$\Delta wAl_2O_3[n] \approx \alpha_1 u_2[n] - \alpha_2 I[n] \tag{31}$$

Notice that equation (27) needs an initial ACD value and this values is not measurable. Indeed, only the ACD variation is calculated by equation (13). This problem can be solved by considering the initial ACD as an additional parameter to be identified.

For $t = NT_s$, equation (27) turns into:

$$\begin{aligned}\Delta R(NT_s) = {} & 2c\Delta wAl_2O_3(NT_s)wAl_2O_3(NT_s) \\ & + d\Delta wAl_2O_3(NT_s) \\ & + e\{\Delta wAl_2O_3(NT_s)[ACD(0) \\ & \quad + \sum_{k=1}^{N} T_s[u_1((k-1)T_s) + \beta I((k-1)T_s))] \\ & \quad + \Delta ACD(NT_s)wAl_2O_3(NT_s)\} \\ & + g\Delta ACD(NT_s)\end{aligned} \tag{32}$$

where:

$$\Delta R(NT_s) := \frac{R(NT_s) - R((N-1)T_s)}{T_s} \tag{33}$$

Defining:

$$\gamma_{1N} := \sum_{k=1}^{N} T_s[u_1((k-1)T_s) + \beta I((k-1)T_s)) \tag{34}$$

Equation (32) becomes:

$$\begin{aligned}\Delta R(NT_s) = {} & 2c\Delta wAl_2O_3(NT_s)wAl_2O_3(NT_s) \\ & + d\Delta wAl_2O_3(NT_s) \\ & + e\{\Delta wAl_2O_3(NT_s)[ACD(0) + \gamma_{1N}] \\ & \quad + \Delta ACD(NT_s)wAl_2O_3(NT_s)\} \\ & + g\Delta ACD(NT_s)\end{aligned} \tag{35}$$

Then, using N samples at $[T_s,\ 2T_s,\ \cdots\ NT_s]$, it is possible to organize equation (32) in a matrix form:

$$\begin{bmatrix}\Delta R(T_s) \\ \vdots \\ \Delta R(NT_s)\end{bmatrix} = \begin{bmatrix}a_{11} & a_{12} & a_{13} & a_{14} \\ \vdots & \vdots & \vdots & \vdots \\ a_{N1} & a_{N2} & a_{N3} & a_{N4}\end{bmatrix} \begin{bmatrix}c \\ d + eACD(0) \\ e \\ g\end{bmatrix} \tag{36}$$

where:

$$\begin{aligned}a_{11} &:= 2\Delta wAl_2O_3(T_s)wAl_2O_3(T_s) \\ a_{12} &:= \Delta wAl_2O_3(T_s) \\ a_{13} &:= \Delta wAl_2O_3(T_s)\gamma_{11} + \Delta ACD(T_s)wAl_2O_3(T_s) \\ a_{14} &:= \Delta ACD(T_s) \\ a_{N1} &:= 2\Delta wAl_2O_3(NT_s)wAl_2O_3(NT_s) \\ a_{N2} &:= \Delta wAl_2O_3(NT_s) \\ a_{N3} &:= \Delta wAl_2O_3(NT_s)\gamma_{1N} + \Delta ACD(NT_s)wAl_2O_3(NT_s) \\ a_{N4} &:= \Delta ACD(NT_s)\end{aligned}$$

Then, the parameters can be identified using a least square estimation algorithm. In Fig. 4, a comparison between the model output and actual measurements is shown. The mean absolute error computed for this data set is 2.21%. However, a small drift can be observed. This happens because the model structure from equation (27) reproduces the resistance variation and needs an initial value.

This difference between the model and the measurements accumulates because of the integrator dynamics inside of the model. Nevertheless, the parameter estimation can be considered valid since the mean absolute error is small.

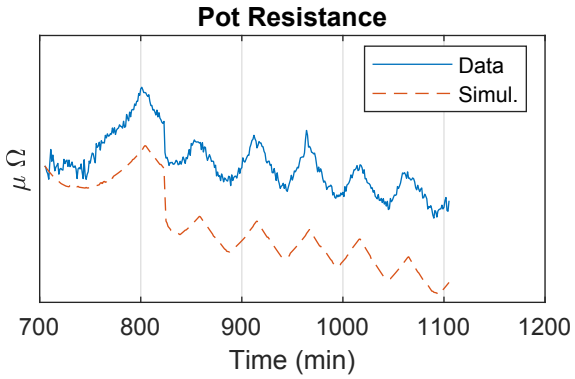

Fig. 4. Resistance Model Validation

4. STATE ESTIMATION

Based on the obtained models for ACD, wAl_2O_3, and R in equations (13), (23), and (27), respectively, and considering the current intensity as a measured disturbance in the system, it is possible to define a discrete-time state-space model of the plant:

$$\begin{cases} \mathbf{x}[n+1] = \begin{bmatrix} 1 & a_{12}[n] & a_{13}[n] \\ 0 & 1 & 0 \\ 0 & 0 & 1 \end{bmatrix} \mathbf{x}[n] + \begin{bmatrix} b_1[n] \\ b_2[n] \\ b_3[n] \end{bmatrix} \\ y[n] = \begin{bmatrix} 1 & 0 & 0 \end{bmatrix} \mathbf{x}[n] \end{cases} \tag{37}$$

where:

$$a_{12}[n] = e(\alpha_1 u_2[n] - \alpha_2 I[n]) \tag{38}$$
$$a_{13}[n] = (2c(\alpha_1 u_2[n] - \alpha_2 I[n]) + e(u_1[n] + \beta I[n]) \tag{39}$$
$$b_1[n] = (d(\alpha_1 u_2[n] - \alpha_2 I[n]) + g(u_1[n] + \beta I[n])) \tag{40}$$
$$b_2[n] = (u_1[n] + \beta I[n]) \tag{41}$$
$$b_3[n] = (\alpha_1 u_2[n] - \alpha_2 I[n]) \tag{42}$$

which all the parameters known and the state vector is:

$$\mathbf{x}[n] = \begin{bmatrix} x_1[n] \\ x_2[n] \\ x_3[n] \end{bmatrix} = \begin{bmatrix} R[n] \\ ACD[n] \\ wAl_2O_3[n] \end{bmatrix} \tag{43}$$

Notice that model (37) is affine in the state. This makes it possible to easily design an observer providing an estimate of the state x by using measurements of the resistance. To perform the state estimation, it is used a Time-Varying Linear Kalman Filter (Kalman, 1960) as a state observer. The Kalman filter equations are given as follows:

Prediction:

$$\hat{\mathbf{x}}[n+1]^- = A[n]\hat{\mathbf{x}}[n] + B[n]$$
$$P[n+1|n] = A[n]P[n|n]A[n]^T + Q_{noise}$$

Update:

$$K[n] = P[n|n-1]C^T(CP[n|n-1]C^T + R_{noise})^{-1}$$
$$\hat{\mathbf{x}}[n] = \hat{\mathbf{x}}[n]^- + K[n](y[k] - C\hat{\mathbf{x}}[n]^-)$$
$$P[n|n] = (I - K[n]C)P[n|n-1]$$

where $\hat{\mathbf{x}}$ is the state estimate vector, P is the covariance, Q_{noise} is the process noise and R_{noise} is the measurement noise matrices. Moreover, the matrices A, B and C come from the state affine system (37):

$$A[n] = \begin{bmatrix} 1 & a_{12}[n] & a_{13}[n] \\ 0 & 1 & 0 \\ 0 & 0 & 1 \end{bmatrix} \tag{44}$$
$$B[n] = [b_1[n]\ b_2[n]\ b_3[n]]^T \tag{45}$$
$$C = [1\ 0\ 0] \tag{46}$$

To implement the observer, it is necessary to tune convariance and noise matrices. The initial covariance matrix $P[0|0]$ is defined as:

$$P[0|0] = \begin{bmatrix} 10^{-1} & 0 & 0 \\ 0 & 10^3 & 0 \\ 0 & 0 & 10^{-1} \end{bmatrix} \tag{47}$$

The largest entry in the P matrix is related to the ACD. As it is not possible to measure this state, we tune the covariance matrix to somehow assign more priority to the estimate of this state. The process and measurement noise matrices, Q_{noise} and R_{noise} respectively are chosen as:

$$Q_{noise} = \begin{bmatrix} 10^{-5} & 0 & 0 \\ 0 & 10^{-5} & 0 \\ 0 & 0 & 10^{-5} \end{bmatrix},\ R_{noise} = 10^{-5} \tag{48}$$

The observer efficiency was tested in two data sets with different initial conditions in order to predict the next states measurements. For each test, it was used a different combination of ACD and wAl_2O_3 initial values in a certain operational range, while the R values were initialized using the actual measurement. The resulting estimates are shown in Fig. 5 and 6, the solid line is the pot resistance measurement, the dashed lines are the states estimations and the "x" markers are the alumina concentration measurements.

In Fig. 5, it is possible to notice a fast convergence, for all estimate independently of the chosen initial condition. Convergence can be verified from the final standard deviation indexes listed in Table 1. The standard deviation of the states R and wAl_2O_3 are smaller than that of the ACD since they are experimentally validated. Fig. 6 shows the estimates provided by the observer for a long period and compare those with the measurements of wAl_2O_3. The values of the mean absolute error reported in Table 1 confirm the effectiveness of the proposed estimation strategy.

Table 1. Estimations Final Values Comparison

	Standard deviation	Mean Absolute Relative Error
R	2.91e-09 $\mu\Omega$	0.09%
ACD	0.0387 cm	-
wAl_2O_3	2.29e-06 %	6.75 %

5. CONCLUSIONS

In this paper, the Hall-Héroult process is modeled by a state affine dynamic system that combines physical-chemical aspects and experimental data. Following this approach, we provide a Linear Kalman filter to estimate the states for the system.

Based on the obtained experimental results, it was possible to validate a state affine model for a complex chemical

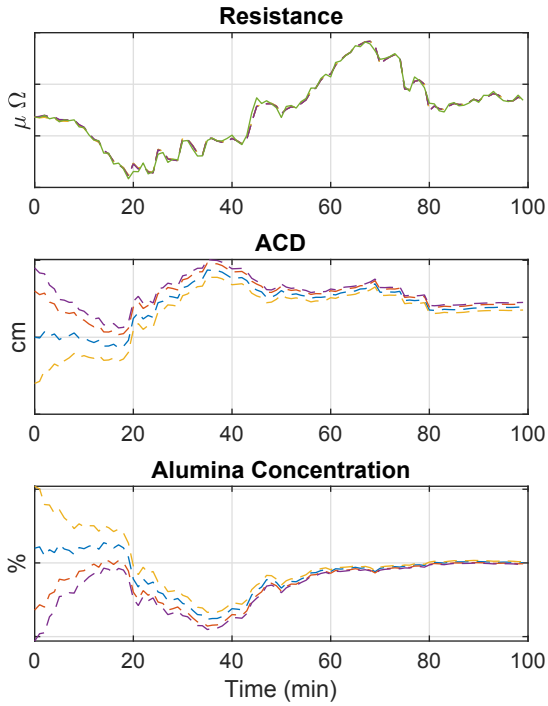

Fig. 5. Data Set 1 - Each dashed line is a state estimation with different initial condition and the solid line is the measurement.

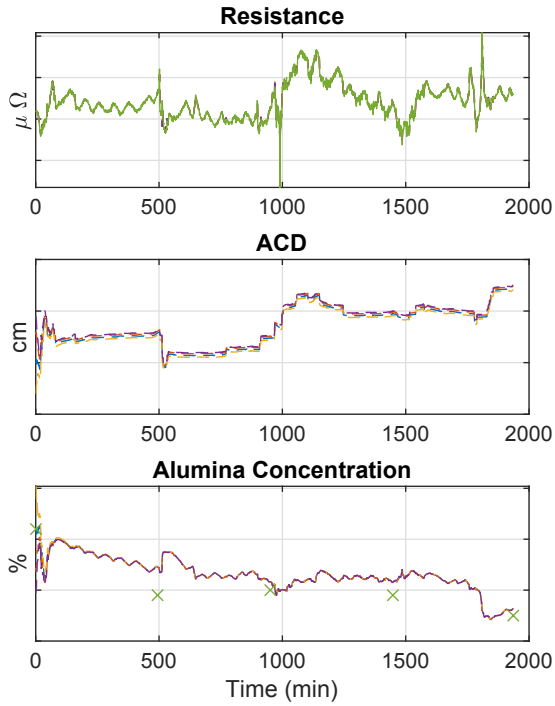

Fig. 6. Data Set 2 - Each dashed line is a state estimation with different initial condition, the solid line and "x" markers are the measurements.

process. Moreover, the chosen observer strategy proved to be reliable by estimating with accuracy the desired states for unknown initial conditions.

ACKNOWLEDGEMENTS

The authors wish to acknowledge project PIANO funded by the French Fonds Unique Interministériel (FUI).

REFERENCES

Bearne, G.P. (1999). The development of aluminum reduction cell process control. *JOM*, 51(5), 16–22.

Côté, P., Martin, O., Allano, B., and Dassylva-Raymond, V. (2017). Predicting instability and current efficiency of industrial cells. In *Light Metals 2017*, 623–629. Springer.

da Silva Moreira, L.J., Besançon, G., Ferrante, F., Fiacchini, M., and Roustan, H. (2020). Model based approach for online monitoring of aluminum production process. In *Light Metals 2020*. Springer.

Grjotheim, K. and Welch, B.J. (1980). *Aluminium Smelter Technology: A Pure and Applied Approach*. Aluminium-Verlag; 2nd edition.

Haupin, W. (2016). Interpreting the components of cell voltage. In *Essential Readings in Light Metals*, 153–159. Springer.

Hestetun, K. and Hovd, M. (2005). Detecting abnormal feed rate in aluminium electrolysis using extended kalman filter. *IFAC Proceedings Volumes*, 38(1), 85–90.

Homsi, P., Peyneau, J.M., and Reverdy, M. (2016). Overview of process control in reduction cells and potlines. In *Essential Readings in Light Metals*, 739–746. Springer.

Jakobsen, S.R., Hestetun, K., Hovd, M., and Solberg, I. (2001). Estimating alumina concentration distribution in aluminium electrolysis cells. *IFAC Proceedings Volumes*, 34(18), 303–308.

Kalman, R.E. (1960). A new approach to linear filtering and prediction problems. *Journal of basic Engineering*, 82(1), 35–45.

Keniry, J.T., Barber, G.C., Taylor, M.P., and Welch, B.J. (2001). Digital processing of anode current signals: an opportunity for improved cell diagnosis and control. *Light Metals*, 1225–1232.

Kolås, S., Foss, B., and Schei, T.S. (2008). State estimation is the real challenge in NMPC. In *International workshop on assessment and future directions of nonlinear model predictive control, Pavia, Italy*.

Moore, J.B. and Anderson, B. (1979). *Optimal filtering*. Prentice-Hall.

Ţiclea, A. and Besançon, G. (2013). Exponential forgetting factor observer in discrete time. *Systems & Control Letters*, 62(9), 756–763.

Yao, Y. and Bao, J. (2018). State and parameter estimation in Hall-Héroult cells using iterated extended Kalman filter. *IFAC-PapersOnLine*, 51(21), 36–41.

Yao, Y., Cheung, C.Y., Bao, J., Skyllas-Kazacos, M., Welch, B.J., and Akhmetov, S. (2017). Estimation of spatial alumina concentration in an aluminum reduction cell using a multilevel state observer. *AIChE Journal*, 63(7), 2806–2818.